Josephson signatures of Weyl node creation and annihilation in irradiated Dirac semimetals

Pei-Hao Fu,[1,2,3] Jun Wang,[4] Jun-Feng Liu [1,2,*] and Rui-Qiang Wang[3,†]

[1]*School of Physics and Electronic Engineering, Guangzhou University, Guangzhou 510006, China*
[2]*Department of Physics, Southern University of Science and Technology, Shenzhen 518055, China*
[3]*Guangdong Provincial Key Laboratory of Quantum Engineering and Quantum Materials, School of Physics and Telecommunication Engineering, South China Normal University, Guangzhou 510006, China*
[4]*Department of Physics, Southeast University, Nanjing 210096, China*

Weyl node creation and annihilation are unique topological phenomena associated with Weyl fermions. Besides the magnetic field, high-frequency illumination can also break the time-reversal symmetry and induce the creation and annihilation of Weyl nodes from a Dirac semimetal. Experimentally, the Weyl node creation and annihilation induced by a magnetic field have been verified by the signature of negative magnetoresistance. In this work, instead of magnetoresistance signatures by application of a magnetic field, we theoretically study the Josephson signatures of Weyl node creation and annihilation in irradiated Dirac semimetals. It is found that Weyl node creation is accompanied by a two-mode oscillation and 0-π transitions in the Josephson current. We further illustrate that two oscillation modes stem from two Andreev reflection processes: opposite-chirality and equal-chirality Andreev reflections, respectively. With Weyl node annihilation, the Josephson current is first shut down and then recovered by the activation of spin-flipping at interfaces by two ferromagnets. The recovered anomalous Josephson current has an arbitrary and tunable ground-state phase difference, other than 0 and π. These predictions are helpful for experimental observation of illumination-induced Weyl node creation and annihilation.

I. INTRODUCTION

Recently, with the achievement of discovering and utilizing topological systems such as graphene [1–3] and topological insulators [4–7], Dirac semimetals (DSMs) [8–15] and Weyl semimetals (WSMs) [16–19] have gained increasing interest and attention. Their unusual transport phenomena [12,16,20–23] all result from the nature of Dirac/Weyl quasiparticles in their band structures, which disperse linearly along all three momentum directions. It is well known that a fourfold degenerate Dirac point is composed of two double-degenerate Weyl points with opposite chiralities. A time reversal (TR)–breaking perturbation, such as a magnetic field, is able to split two spin subbands so as to create a pair of Weyl nodes from each Dirac node [24].

The creation and annihilation of Weyl nodes are unique properties of WSMs. Experimentally, in DSMs, the observation of negative magnetoresistance confirms the creation of Weyl nodes under a magnetic field [25–27]. Such a negative magnetoresistance serves as a characteristic transport signature of WSMs and is a direct result of a chiral anomaly [23] which is caused by charge pumping between a pair of Weyl nodes under parallel electric and magnetic fields. These observations as well as the recently discovered breakdown of a chiral anomaly [28–32] in a high magnetic field are

the magnetotransport signatures of Weyl node creation and annihilation.

Instead of the application of a magnetic field, Weyl nodes in DSMs can be created by high-frequency illumination. Actually, through Floquet theory [33,34], a Floquet-Weyl semimetal (FWSM) can be realized and the positions of Weyl nodes in momentum space can be shifted in irradiated systems [34–41], including three-dimensional (3D) topological insulators [34], nodal-line semimetals [35–38], and DSMs (see Fig. 2) [35,36,39,40]. Furthermore, with a high driving amplitude, Weyl node annihilation has also been predicted in irradiated DSMs [40]. It is demonstrated that a system possesses a so-called spin-polarized Weyl semimetal (SP-WSM) phase, where one pair of Weyl nodes with one spin is annihilated first, with the remaining pair of Weyl nodes having opposite spin. For a higher driving amplitude, the remaining pair of Weyl nodes can also be annihilated. The interaction between light and matter provides us another path to the efficient creation and annihilation Weyl nodes in 3D materials.

In this paper, to observe such illumination-induced Weyl node creation and annihilation in transport experiments, we theoretically investigate the Josephson signatures in irradiated DSMs, instead of magnetoresistance signals caused by an external magnetic field. Previously, there have been extensive theoretical and experimental efforts focusing on the interplay between superconductors (SCs) and DSMs or WSMs [42–59]. It has been indicated that the Josephson current oscillates as a result of a change in the distance between two paired Weyl nodes, which is tunable by linearly polarized light [42–44].

*phjfliu@gzhu.edu.cn
†rqwanggz@163.com

The origin is that only an equal-chirality Andreev reflection (AR) is permitted at the interface between a magnetic WSM and an *s*-wave SC because of the opposite-spin pairing, which endows the Cooper pair in the WSM with an extra net momentum. The chirality blockage of the AR in a magnetic WSM has also been predicted when the magnetization lies in the plane of the WSM-SC interface [45]. However, the Josephson signal of Weyl node creation and annihilation has rarely been studied yet. We study the Josephson effect in a DSM where Floquet-Weyl nodes are created, shifted, and annihilated by high-frequency circularly polarized light. It is found that the creation of Weyl nodes due to spin splitting leads to two-mode oscillations and 0-π transitions in the Josephson current. We further illustrate that two oscillation modes stem from two AR processes, opposite-chirality and equal-chirality Andreev reflections, respectively. When right-handed (left-handed) circularly polarized light is applied, the spin-up (spin-down) pair of Weyl nodes is first annihilated with an increasing light amplitude. In this SPWSM phase, the Josephson current is shut down because the opposite-spin AR is forbidden. If the spin-flipping process is activated at SPWSM-SC interfaces by two ferromagnets (FMs), the Josephson current can be recovered. The current-phase relation can have an arbitrary ground-state phase difference [60–65], other than 0 and π. It is tunable by the angle between the magnetization orientations of two FMs. When the second pair of Weyl nodes is also annihilated by the higher amplitude of the driving field, the Josephson current is totally shut down.

This paper is organized as follows. The tight-binding model Hamiltonian of DSMs with illumination as well as the method for calculating the Josephson current and Andreev bound states (ABSs) is introduced in Sec. II. Our main numerical results for Josephson signals and related discussion are given in Sec. III, including the two-mode oscillation and 0-π phase transition accompanying Weyl node creation and the anomalous Josephson effect accompanying the annihilation of the first pair of Weyl nodes. A brief summary is given in Sec. IV.

II. MODEL AND FORMALISM

The relevant setup, as depicted in Fig. 1, consists of a light-dressed DSM sandwiched by two FMs and then two *s*-wave SC leads which are characterized by different macroscopic
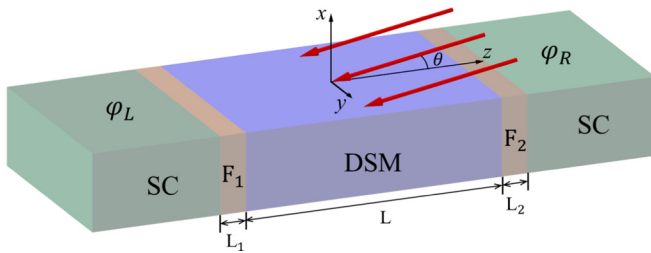
FIG. 1. The Josephson junction of an irradiated DSM of length L, sandwiched by two ferromagnets ($F_{\alpha=1,2}$) of length L_α and two *s*-wave SCs characterized by macroscopic phases labeled $\varphi_{j=L/R}$. Parallel red arrows denote incident light in the *x*-*z* plane with the azimuth angle θ measured from the *z* axis.

TABLE I. Parameters for Cd$_3$As$_2$ from the *ab initio* calculation [24].

A	0.889 eV Å
C_0	−0.0145 eV
C_z	10.59 eV Å^2
$C_x = C_y$	11.5 eV Å^2
M_0	−0.0205 eV
M_z	−18.77 eV Å^2
$M_x = M_y$	−13.5 eV Å^2

phases $\varphi_{L/R}$. We begin with the low-energy effective Hamiltonian of a DSM around the Γ point in the basis $\{|S_{J=1/2}, J_z = 1/2\rangle, |P_{3/2}, 3/2\rangle, |S_{1/2}, -1/2\rangle, |P_{3/2}, -3/2\rangle\}$,

$$H(\boldsymbol{k}) = \begin{pmatrix} H_+(\boldsymbol{k}) & 0 \\ 0 & H_-(\boldsymbol{k}) \end{pmatrix}, \quad (1)$$

where $H_\sigma(\boldsymbol{k}) = \epsilon_0(\boldsymbol{k})\tau_0 + A(\sigma k_x \tau_x - k_y \tau_y) + M(\boldsymbol{k})\tau_z$, with $\epsilon_0(\boldsymbol{k}) = C_0 + \sum_{i=x,y,z} C_i k_i^2$ and $M(\boldsymbol{k}) = M_0 - \sum_i M_i k_i^2$. τ_0 and $\tau_{x,y,z}$ are the unit matrix and Pauli matrices for the orbital degree of freedom, while $\sigma = +/-$ denotes spin-up/spin-down subbands. This Hamiltonian is valid for Cd$_3$As$_2$ and Na$_3$Bi. In this work, we take Cd$_3$As$_2$ as an example and the parameters from the *ab initio* calculation are listed in Table I [24]. By solving the Hamiltonian, we can find two Dirac nodes located at $\boldsymbol{K}_D = (0, 0, \pm\sqrt{M_0/M_z})$ in the spectrum as depicted in Fig. 2(a). To calculate the Josephson current using the lattice Green's function technique, we rewrite this Hamiltonian as a tight-binding one in the cubic lattice by substituting k_i and k_i^2 with $a_i^{-1}\sin k_i a_i$ and $2a_i^{-2}(1 - \cos k_i a_i)$, respectively, where a_i are the lattice constants in the i direction and they are set to be $a_x = a_y = a_z = a = 20$ Å [47].

As has been reported, abundant phases can be realized in periodically driven DSMs by high-frequency light [35,36,40,41]. A driving field in the *x*-*z* plane can be written as a time-dependent vector potential,

$$\boldsymbol{A}(t_l) = (A_x \cos \omega t_l, A_y \sin(\omega t_l + \phi), A_z \cos \omega t_l), \quad (2)$$

with the components $A_x = (E_0/\omega)\cos\theta$, $A_y = E_0/\omega$, and $A_z = -(E_0/\omega)\sin\theta$. Here E_0 is the strength of the electric component of the electromagnetic wave whose frequency is ω, θ is the azimuth angle measured from the z axis, and ϕ represents light polarization. $\phi = 0$ (π) corresponds to right-handed (left-handed) circularly polarized light, and $\phi = \pm\pi/2$ to linearly polarized light. In the presence of illumination, the irradiated system is described in terms of a time-dependent Hamiltonian $H(\boldsymbol{k}, t_l)$ by the Peierls substitution, $\boldsymbol{k} \rightarrow \boldsymbol{k} + e\boldsymbol{A}(t_l)/\hbar$. Hereafter, we use natural units with $\hbar = 1 = e$ and $A_0 \equiv eE_0(\hbar\omega)^{-1}$ to renormalize the amplitude of the driving field. In the high-frequency limit, where the energy of incident photon $\hbar\omega$ is much higher than other characteristic energy scales in the system, an effective Hamiltonian takes the form [33,34]

$$H_{\text{eff}}(\boldsymbol{k}) = H_0(\boldsymbol{k}) + \sum_{n>0} \frac{[H_{+n}(\boldsymbol{k}), H_{-n}(\boldsymbol{k})]}{n\omega} + \hat{O}\left(\frac{1}{\omega^2}\right), \quad (3)$$
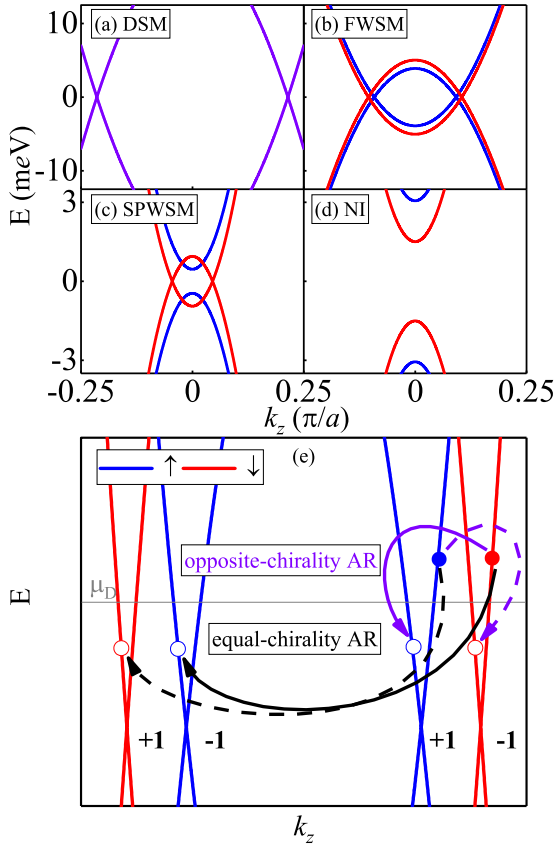
FIG. 2. (a–d) Band structures of an DSM irradiated by a right-handed circularly polarized light with various driving amplitudes: $A_0 = 0$ (a), $A_0 = 0.035\,\text{Å}^{-1}$ (b), $A_0 = 0.0395\,\text{Å}^{-1}$ (c), and $A_0 = 0.042\,\text{Å}^{-1}$ (d). (e) Schematic of opposite- and equal-chirality ARs in the FWSM phase with a chemical potential μ_D where the solid (dashed) violet arrow denotes the opposite-chirality AR from spin-down (spin-up) electrons to spin-up (spin-down) holes, while the solid and dashed black arrows represent the equal-chirality ARs. The labels ± 1 in (e) represent the chirality of Weyl nodes, i.e., $\chi_\pm^\sigma = \pm \sigma$. In (a)–(e), spin-up (spin-down) subbands are plotted by blue (red) lines.

where $H_n(\mathbf{k}) = \frac{1}{T_l}\int_{-T_l/2}^{T_l/2} dt_l H(\mathbf{k}, t_l)e^{-in\omega t_l}$ are the Fourier components of the time-dependent Hamiltonian with period $T_l = 2\pi/\omega$. After some algebra, the light-dressed effective tight-binding Hamiltonian is

$$H'(\mathbf{k}) = \begin{pmatrix} H'_+(\mathbf{k}) & 0 \\ 0 & H'_-(\mathbf{k}) \end{pmatrix}, \tag{4}$$

with $H'_\sigma(\mathbf{k}) = H_{0,\sigma}(\mathbf{k}) + H_{L,\sigma}(\mathbf{k})$. The first term is

$$H_{0,\sigma}(\mathbf{k}) = \tilde{\epsilon}_k \tau_0 + \tilde{M}_k \tau_z + \sigma \tilde{A}_x \sin k_x a \tau_x - \tilde{A}_y \sin k_y a \tau_y, \tag{5}$$

which has a form similar to that of H_σ, but with light-dressed parameters:

$$\tilde{\epsilon}_k = C_0 + 2a^{-2}\sum_i C_i[1 - J_0(A_i a)\cos k_i a],$$

$$\tilde{M}_k = M_0 - 2a^{-2}\sum_i M_i[1 - J_0(A_i a)\cos k_i a],$$

$$\tilde{A}_{x(y)} = J_0(A_{x(y)}a)Aa^{-1}. \tag{6}$$

The second term is

$$H_{L,\sigma}(\mathbf{k}) = A'\tau_x \cos k_y a \sin k_x a - \sigma A'\tau_y \cos k_x a \sin k_y a$$
$$+ \sigma M'_0 \tau_z \cos k_x a \cos k_y a + \zeta \tau_x \cos k_y a \sin k_z a, \tag{7}$$

with

$$A' = 8J_1(A_x a)J_1(A_y a)(\omega a^3)^{-1}AM_x \cos\phi,$$

$$\zeta = 8J_1(A_y a)J_1(A_z a)(\omega a^3)^{-1}AM_z \cos\phi,$$

$$M'_0 = 4J_1(A_x a)J_1(A_y a)(\omega a^2)^{-1}A^2 \cos\phi, \tag{8}$$

where $J_n(x)$ is the nth-order Bessel function and the terms $J_{n>1}(x)$ have been neglected due to the high-frequency approximation.

By applying a right-handed/left-handed circularly polarized light with a nonzero M'_0, the TR symmetry is broken and the system enters a FWSM phase upon the splitting of each Dirac node into a pair of Floquet-Weyl nodes [40]. In the limit of $\theta \to 0$, the light-dressed band structure holds two pairs of Floquet-Weyl nodes, located at $\mathbf{K}_W^\sigma = (0, 0, \pm k_0^\sigma)$, as shown in Figs. 2(a)–2(d), with $k_0^\sigma = a^{-1}\arccos\{[2a^{-2}M_z J_0(A_z a)]^{-1}(\tilde{M}_0 + \sigma M'_0)\}$ and $\tilde{M}_0 = M_0 + 2a^{-2}M_x J_0(A_x a) + 2a^{-2}M_y J_0(A_y a) - 2a^{-2}\sum_i M_i$. It is also noticeable that the chiralities of Floquet-Weyl nodes are locked with spin, i.e., $\chi_\pm^\sigma = \pm\sigma$, as shown in Fig. 2(e). With increasing driving amplitude, one pair of Floquet-Weyl nodes with one spin is first annihilated. The remaining pair of Weyl nodes with the other spin forms an SPWSM phase. When $\theta \neq 0$, the locations of Floquet-Weyl nodes will slightly deviate from the k_z axis due to a nonzero ζ but the deviation is much smaller than the splitting along the k_z axis [40].

To study the transport signature of Weyl node creation and annihilation, a Josephson junction mediated by an irradiated DSM is investigated, as shown in Fig. 1. Because the junction is translationally invariant along the x and y directions, we only discretize the system along the z direction to use the lattice Green's function technique for calculation of the Josephson current [46]. The discretized Bogoliubov–de Gennes Hamiltonian in the DSM region takes the form

$$H_D = \sum_{i,\mathbf{k}_\parallel} (\phi^\dagger_{i,\mathbf{k}_\parallel} \quad \phi_{i,-\mathbf{k}_\parallel}) \begin{pmatrix} h_D(\mathbf{k}_\parallel) + h_L(\mathbf{k}_\parallel) - \mu_D & 0 \\ 0 & -h_D^*(-\mathbf{k}_\parallel) - h_L^*(-\mathbf{k}_\parallel) + \mu_D \end{pmatrix} \begin{pmatrix} \phi_{i,\mathbf{k}_\parallel} \\ \phi^\dagger_{i,-\mathbf{k}_\parallel} \end{pmatrix}$$

$$+ \sum_{i,\mathbf{k}_\parallel} \left[(\phi^\dagger_{i,\mathbf{k}_\parallel} \quad \phi_{i,-\mathbf{k}_\parallel}) \begin{pmatrix} \hat{t}_z & 0 \\ 0 & -\hat{t}_z^* \end{pmatrix} \begin{pmatrix} \phi_{i+1,\mathbf{k}_\parallel} \\ \phi^\dagger_{i+1,-\mathbf{k}_\parallel} \end{pmatrix} + \text{H.c.} \right], \tag{9}$$

where i is the site index along the z direction, $\phi_{i,\boldsymbol{k}_\parallel} = [c_{i,S\uparrow,\boldsymbol{k}_\parallel}, c_{i,P\uparrow,\boldsymbol{k}_\parallel}, c_{i,S\downarrow,\boldsymbol{k}_\parallel}, c_{i,P\downarrow,\boldsymbol{k}_\parallel}]^T$ is the field operator in the DSM, with $c_{i,S(P)\uparrow(\downarrow),\boldsymbol{k}_\parallel}$ ($c_{i,S(P)\uparrow(\downarrow),\boldsymbol{k}_\parallel}^\dagger$) being the annihilation (creation) operator of the S (P) orbit electron at site i with spin $\uparrow$ ($\downarrow$) and parallel momentum $\boldsymbol{k}_\parallel = (k_x, k_y)$, μ_D is the chemical potential, and the matrix components are

$$h_D(\boldsymbol{k}_\parallel) = \begin{pmatrix} H_{0,+}(k_z = \pi/2a) & 0 \\ 0 & H_{0,-}(k_z = \pi/2a) \end{pmatrix},$$

$$h_L(\boldsymbol{k}_\parallel) = \begin{pmatrix} H_{L,+}(k_z = 0) & 0 \\ 0 & H_{L,-}(k_z = 0) \end{pmatrix}, \quad (10)$$

and

$$\hat{t}_z = \sigma_0[J_0(A_z a)(C_z\tau_0 - M_z\tau_z) + i\zeta/2\cos(k_y a)\tau_x], \quad (11)$$

where σ_0 and $\boldsymbol{\sigma}$ are the unit matrix and the Pauli matrices in spin space, respectively.

The SC leads are described by the Hamiltonian as

$$H_S = \sum_{j,i,\boldsymbol{k}_\parallel} \psi_{i,\boldsymbol{k}_\parallel}^\dagger \begin{pmatrix} h_S(\boldsymbol{k}_\parallel)\sigma_0 & e^{i\varphi_j}\Delta i\sigma_y \\ -e^{-i\varphi_j}\Delta i\sigma_y & -h_S^*(-\boldsymbol{k}_\parallel)\sigma_0 \end{pmatrix} \psi_{i,\boldsymbol{k}_\parallel}$$

$$+ \sum_{j,i,\boldsymbol{k}_\parallel} \left[\psi_{z,\boldsymbol{k}_\parallel}^\dagger \begin{pmatrix} t\sigma_0 & 0 \\ 0 & -t\sigma_0 \end{pmatrix} \psi_{i+1,\boldsymbol{k}_\parallel} + \text{H.c.} \right], \quad (12)$$

where $\psi_{i,\boldsymbol{k}_\parallel} = [c_{i,\uparrow,\boldsymbol{k}_\parallel}, c_{i,\downarrow,\boldsymbol{k}_\parallel}, c_{i,\uparrow,-\boldsymbol{k}_\parallel}^\dagger, c_{z,\downarrow,-\boldsymbol{k}_\parallel}^\dagger]^T$ is the field operator in SC leads, $h_S(\boldsymbol{k}_\parallel) = -\mu_S - 2t\sum_{i=x,y}\cos k_i a$, with μ_S the chemical potential, $j = L(R)$ denoting the left (right) SC lead with the macroscopic phase φ_j, and nearest-neighbor hopping t. Similarly, the FMs are described by

$$H_F = \sum_{\alpha,i,\boldsymbol{k}_\parallel} \psi_{i,\boldsymbol{k}_\parallel}^\dagger \begin{pmatrix} h_F(\boldsymbol{k}_\parallel) & 0 \\ 0 & -h_F^*(-\boldsymbol{k}_\parallel) \end{pmatrix} \psi_{i,\boldsymbol{k}_\parallel}$$

$$+ \sum_{\alpha,i,\boldsymbol{k}_\parallel} \left[\psi_{i,\boldsymbol{k}_\parallel}^\dagger \begin{pmatrix} t\sigma_0 & 0 \\ 0 & -t\sigma_0 \end{pmatrix} \psi_{i+1,\boldsymbol{k}_\parallel} + \text{H.c.} \right], \quad (13)$$

where $h_F(\boldsymbol{k}_\parallel) = h_S(\boldsymbol{k}_\parallel)\sigma_0 + \boldsymbol{h}_\alpha \cdot \boldsymbol{\sigma}$ and α is the index counting two FMs. The exchange field $\boldsymbol{h}_\alpha = h_{0\alpha}(\sin\theta_{m\alpha}\cos\varphi_{m\alpha}, \sin\theta_{m\alpha}\sin\varphi_{m\alpha}, \cos\theta_{m\alpha})$ with strength $h_{0\alpha}$ and magnetization orientation $(\theta_{m\alpha}, \varphi_{m\alpha})$.

The coupling between the DSM and two FMs is

$$H_C = \sum_{i,\boldsymbol{k}_\parallel} [(\phi_{i,\boldsymbol{k}_\parallel}^\dagger, \phi_{i,-\boldsymbol{k}_\parallel})h_c\psi_{i,\boldsymbol{k}_\parallel} + \text{H.c.}], \quad (14)$$

where $h_c = \nu_z \otimes \sigma_0 \otimes (t_s, t_p)^T$ is an 8×4 matrix, with ν_z being the third Pauli matrix in electron-hole space. The hopping energies for s- and p-orbital electrons are denoted t_s and t_p, respectively. For simplicity, we assume $t_s = t_p = t$, which can be controlled by barriers in experiments [68]. Our numerical results verify that the Josephson current is not sensitive to modest differences between t_s and t_p. The coupling between FMs and SC leads is the same with the nearest-neighbor hopping matrix in FMs and SC leads $H_{\text{FS}} = t\nu_z \otimes \sigma_0$.

Thus, the whole Josephson junction is captured by the Hamiltonian $H = H_D + H_F + H_S + H_C + H_{\text{FS}}$. Using the lattice Green's function technique, the Josephson current through column l in the driven DSM region for a given $\boldsymbol{k}_\parallel$

is calculated by [46]

$$J(\boldsymbol{k}_\parallel) = \frac{1}{h} \int_{-\infty}^{\infty} \text{Tr}[T_z^\dagger \hat{e} G_{l,l-1}^<(\boldsymbol{k}_\parallel) - \hat{e} T_z G_{l-1,l}^<(\boldsymbol{k}_\parallel)]dE, \quad (15)$$

where $T_z = \begin{pmatrix} \hat{t}_z & 0 \\ 0 & -\hat{t}_z^* \end{pmatrix}$ and $\hat{e} = -ev_z\sigma_0\tau_0$ is the charge matrix. At equilibrium, the lesser-than Green's function is calculated by $G^< = f(E)[G^a - G^r]$, where $f(E)$ is the Fermi-Dirac distribution function. The retarded (advanced) Green's function $G^{r(a)}$ reads

$$G^r(E) = [G^a(E)]^\dagger = \frac{1}{E - H_d - \Sigma_L^r(E) - \Sigma_R^r(E)}, \quad (16)$$

where H_d is the Hamiltonian of the whole device region including the DSM and two FMs, and the retarded self-energy $\Sigma_{L/R}^r(E)$ representing the coupling with the left/right SC lead can be calculated numerically by the recursive method [66,67]. Finally, the total Josephson current is given by $I = \sum_{\boldsymbol{k}_\parallel} J(\boldsymbol{k}_\parallel)$.

In addition, to understand the behavior of the Josephson current, one can calculate ABS spectra through the Green's function technique numerically. The energies of ABS levels can be located by searching the peaks of particle density within the SC gap at column l ($1 \leqslant l \leqslant L$),

$$\rho_l = -\frac{1}{\pi} \text{Im}[\text{Tr}G_{l,l}^r], \quad (17)$$

at a given phase difference $\varphi = \varphi_R - \varphi_L$.

III. RESULTS AND DISCUSSION

A. Weyl node creation

In this section, we present the numerical results for the band structure of an irradiated DSM and the Josephson current through the junction. In the numerical calculation, we use the parameters for Cd$_3$As$_2$ mentioned above but set $C_{0,x,y,z} = 0$ to ignore the energy shift of Dirac/Weyl points caused by the driving field. This is reasonable because $C_{0,x,y,z}$ do not change the location of Weyl nodes and the energy shift of the Weyl nodes can be compensated by the self-tuning of the chemical potential μ_D. We consider a junction of considerable sizes along the x and y directions and choose a chemical potential moderately far from the Dirac points to ignore the effect of Fermi arc surface states. It is also noticeable that Fermi arc surface states are dispersionless along the k_z direction. This means that the surface states make no contribution to the transport when the junction is along the z direction.

For SC leads, the zero-temperature superconducting gap is $\Delta_0 = t/500 = 0.135$ meV, and the gap at a finite temperature T is $\Delta = \Delta_0 \tanh(1.74\sqrt{T_c/T - 1})$, where T_c is the critical temperature. In our calculations, the chemical potential is the same in both SC leads and FMs, $\mu_S = -4.4t$. The nearest-neighbor hopping $t \equiv |2M_x a^{-2}|$ is the same as the transverse hopping in the DSM, for simplicity. We argue that the detailed parameters in SC leads should not change the supercurrent qualitatively, which should be mainly determined by the positions of Weyl nodes and have been verified by the numerical results. To ensure that the high-frequency limit is a good approximation, the energy of the incident photon is set to be
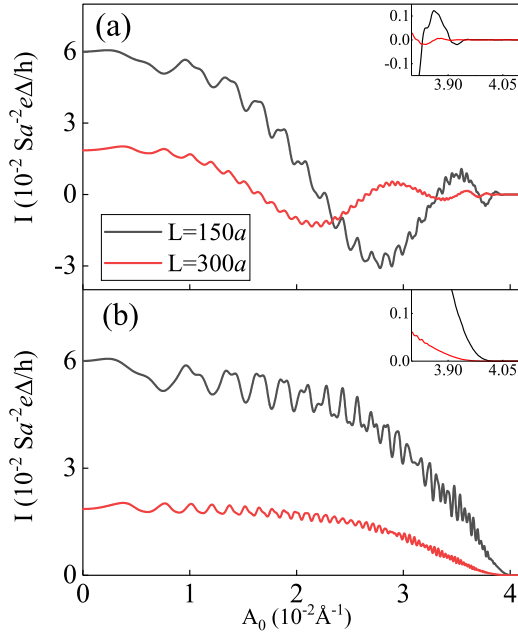
FIG. 3. The Josephson current at $\varphi = \pi/2$ as a function of the driving amplitude of (a) a right-handed circularly polarized light or (b) a linearly polarized light. In units of I, S is the cross-section area of the junction in the x-y plane. The temperature is $T = 0.5T_c$ and the chemical potential is $\mu_D = 5\Delta_0$. $L_1 = L_2 = 0$. Insets: Decay of the current around $A_1^c \approx 0.039 \ \text{Å}^{-1}$ and $A_2^c \approx 0.041 \ \text{Å}^{-1}$.

$\hbar\omega = 1.5$ eV, which is much higher than the characteristic energy of electrons.

Figures 2(a)–2(d) show the band structures of an irradiated DSM with various amplitudes of the circularly polarized driving field with $\theta = 0 = \phi$. With an increasing driving amplitude, the evolution of the band structure clearly manifests the creation and annihilation of Weyl nodes from the DSM. Two critical values of the driving amplitude for Weyl node annihilation should be noted: $A_1^c \approx 0.039 \ \text{Å}^{-1}$ and $A_2^c \approx 0.041 \ \text{Å}^{-1}$. The system is an FWSM for $0 < A_0 < A_1^c$, an SPWSM for $A_1^c < A_0 < A_2^c$, and a normal insulator (NI) for $A_2^c < A_0$. All the parameters are accessible in current experiments [69–71].

In the following, we consider only the limit case with $\theta \to 0$ in the calculation of the Josephson current. This means that only the light incident from the z direction is considered. We argue that the light incident from the x (y) direction causes only a much smaller shift of Weyl nodes in the k_x (k_y) direction [40] and has little effect on the Josephson current.

We first check the Josephson signature of Weyl node creation. For this purpose, two FMs are not necessary and we set $L_1 = L_2 = 0$. Figure 3(a) plots the Josephson current at $\varphi = \pi/2$ through an irradiated DSM by a right-handed circularly polarized light as a function of the amplitude of the driving field. Note that the current at $\varphi = \pi/2$ is approximately equivalent to the critical current for the temperature $T = 0.5T_c$, where the current-phase relation is nearly sinusoidal as shown in Fig. 5(a). With increasing driving amplitude, the current exhibits a two-mode near-periodic oscillation. It is noticeable that the long-period mode oscillation even reverses the Josephson current and induces a 0-π transition. This 0-π

transition is attributed to spin-splitting-induced Weyl node creation as discussed below. In contrast, the 0-π transition is absent in the case of linearly polarized light [see Fig. 3(b)], where Weyl node creation is also absent due to the preserved TR symmetry. But the short-period mode oscillation remains due to the shift of Dirac nodes in the irradiated DSM by a linearly polarized light. Besides, as shown in the inset in Fig. 3, the Josephson current for the circularly polarized light vanishes when $A_0 > A_1^c$, where the pair of spin-up Weyl nodes is annihilated and the DSM becomes an SPWSM such that the spin-flip AR is not possible. But the Josephson current for the linearly polarized light is maintained until $A_0 > A_2^c$ where the system is gapped.

To understand the two-mode oscillation and 0-π transitions, we consider the ARs at the DSM-SC interface. For a fixed chemical potential μ_D, the four positive wave vectors in the band structure of the DSM are

$$k_\sigma^\pm = a^{-1} \arccos \left[\frac{\tilde{M}_0 + \sigma M_0' \pm \mu}{-2J_0(A_z a)a^{-2}M_z} \right], \quad (18)$$

where σ denotes the spin and the sign $+$ $(-)$ denotes the right-going (left-going) wave. As sketched in Fig. 2(e), both opposite-chirality ARs and equal-chirality ARs can occur at the interface. The (equal-chirality) opposite-chirality ARs make a Cooper pair of two electrons from two Weyl nodes with (equal) opposite chiralities. For the opposite-chirality AR, the net momentum of the Cooper pair is nearly $\pm(k_0^\uparrow + k_0^\downarrow)$, which induces a phase shift $\pm(k_0^\uparrow + k_0^\downarrow)L$ in the current-phase relation. For the equal-chirality AR, the net momentum of the Cooper pair is nearly $\pm(k_0^\uparrow - k_0^\downarrow)$, which induces a phase shift $\pm(k_0^\uparrow - k_0^\downarrow)L$. Thus, the total Josephson current can be written as

$$J = [c_1 \cos(k_0^\uparrow + k_0^\downarrow)L + c_2 \cos(k_0^\uparrow - k_0^\downarrow)L] \sin\varphi, \quad (19)$$

where the amplitudes c_1 and c_2 depend on the probabilities of two kinds of ARs. This expression can well explain the two-mode oscillation and 0-π transitions in the case of circularly polarized light. For the linearly polarized light, spin splitting and Weyl node creation are absent, i.e., $k_0^\uparrow = k_0^\downarrow$, thus the long-period oscillation vanishes and only the short-period oscillation remains. The 0-π transition is also absent due to the fact that $c_1 \approx c_2$. Therefore, we can consider the two-mode oscillation and 0-π transitions to be the Josephson signatures of Weyl node creation in irradiated DSMs.

To numerically verify the validity of Eq. (19), we plot the Josephson current at $\varphi = \pi/2$ as the function of the length L in Fig. 4(a) for the situation of circularly polarized light. The two-mode periodic oscillation with increasing L is clearly exhibited in the current. The corresponding Fourier frequency spectrum shown in Fig. 4(b) also confirms two typical frequencies. The lower frequency agrees exactly with the momentum of the Cooper pair formed by equal-chirality ARs, $\delta k_2 = |k_\uparrow^+ - k_\downarrow^+| \approx |k_0^\uparrow - k_0^\downarrow|$, as shown in Fig. 4(c). Similarly, the higher frequency agrees with the momentum of the Cooper pair formed by opposite-chirality ARs, $\delta k_{1,\uparrow(\downarrow)} = |k_{\uparrow(\downarrow)}^+ + k_{\downarrow(\uparrow)}^-| \approx |k_0^\uparrow + k_0^\downarrow|$. Finally, the 0-$\pi$ transitions with increasing driving amplitude are also confirmed by both the current-phase relation and the ABS levels shown in Figs. 5(a) and 5(b).
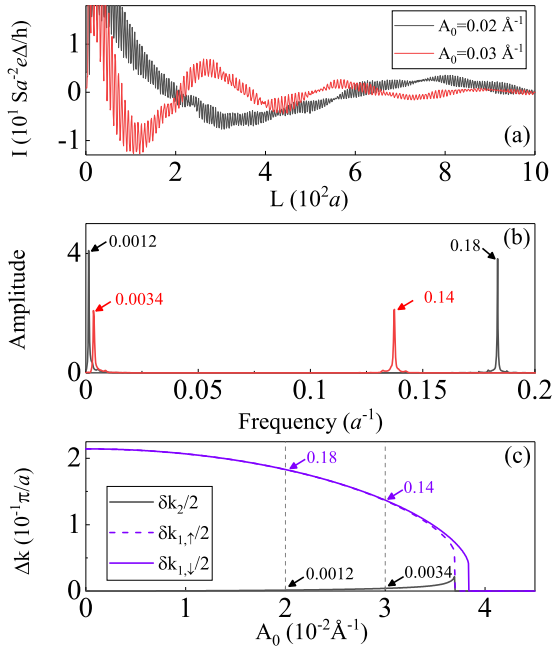
FIG. 4. (a) The Josephson current at $\varphi = \pi/2$ as a function of the length L for two fixed driving amplitudes. (b) The corresponding Fourier frequency spectrum. (c) The net momenta of Cooper pairs formed by equal- and opposite-chirality ARs sketched in Fig. 2(e). The temperature is $T = 0.1T_c$ and the other parameters are the same as in Fig. 3.

B. Weyl node annihilation

When the driving amplitude increases up to the region $A_1^c < A_0 < A_2^c$, the pair of spin-up Weyl nodes is annihilated and the DSM enters an SPWSM phase. The Josephson current
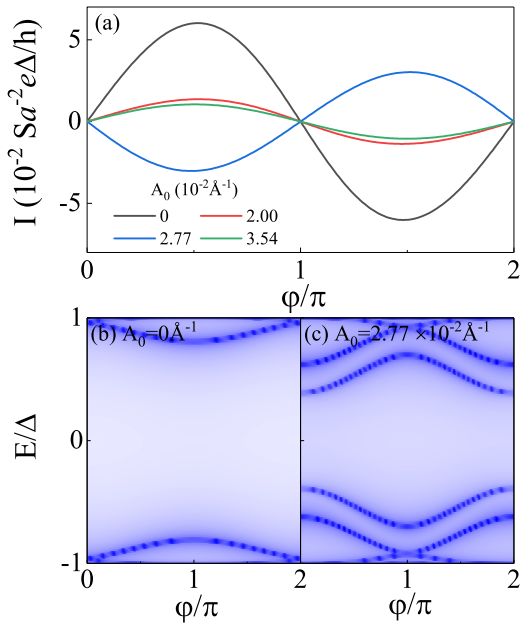
FIG. 5. The current-phase relation of (a) the Josephson current and (b,c) the Andreev bound states at various driving amplitudes. Other parameters are the same as in Fig. 3.
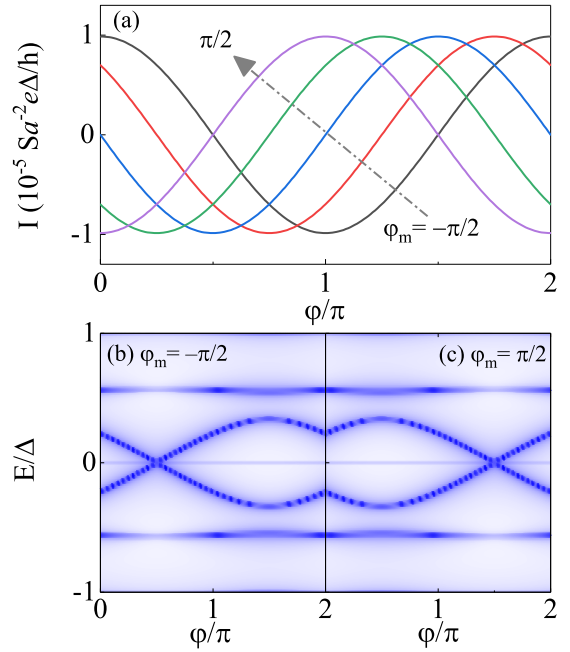
FIG. 6. (a) The current-phase relation of the Josephson junction with various relative magnetization angles $\varphi_m = \varphi_{m2} - \varphi_{m1}$, which change from $-\pi/2$ to $\pi/2$ with a step of $\pi/4$ when two FM layers are activated. (b, c) The Andreev bound states for $\varphi_m = -\pi/2$ (b) and $\varphi_m = \pi/2$ (c). $\theta_{m1} = \theta_{m2} = \pi/2$ and $\varphi_{m1} = 0$. $h_{01} = h_{02} = 0.05t$ and $L_1 = L_2 = 29a$. The driving amplitude is $A_0 = 0.0395$ Å^{-1}, which means that the DSM is in an SPWSM phase. $L = 150a$, $\mu_D = 2\Delta_0$, and other parameters are the same as in Fig. 3.

vanishes in the absence of two FMs since the opposite-spin AR is forbidden. When two FMs are activated, the Josephson current can be recovered due to the spin flipping or spin precession by two FMs. To precess the spin, we set $\theta_{m1} = \theta_{m2} = \pi/2$. The current is maximum when the precession angle is $\pi/2$ in a single trip and thus π in a round trip. The precession angle in the αth FM is evaluated by $(k_{\alpha+} - k_{\alpha-})L_\alpha$, where $k_{\alpha+}$ ($k_{\alpha-}$) is the wave vector of the electron or hole with spin parallel (antiparallel) to the spin quantization axis of the FM.

Figure 6(a) plots the current-phase relation for various relative magnetization angles $\varphi_m = \varphi_{m2} - \varphi_{m1}$ when two FM layers are activated. With parameters $h_{01} = h_{02} = 0.05t$ and $L_1 = L_2 = 29a$, we have the precession angle $(k_{\alpha+} - k_{\alpha-})L_\alpha \approx \pi/2$ for both FMs. The current-phase relations exhibit an anomalous phase shift $-\pi$-φ_m compared with a sinusoidal one, which is similar to the situation of an anomalous Josephson current through a noncoplanar ferromagnetic trilayer [60]. This anomalous Josephson effect stems from the broken symmetries including both the TR and the spin rotation or chiral symmetry [61]. Figures 6(b) and 6(c) show the ABSs for $\varphi_m = -\pi/2$ and $\pi/2$, respectively. The ABSs clearly confirm the phase shift and are consistent with the corresponding current-phase relations. Thus it can be seen that the unique SPWSM phase in an irradiated DSM provides a platform for engineering an anomalous Josephson φ_0 junction with a tunable ground-state phase difference. When the driving amplitude exceeds A_2^c, the remaining pair of spin-down

Weyl nodes will also be annihilated and the DSM enters a normal insulator phase. The Josephson current will be totally blocked.

C. Discussion

Although we consider only the limit case with $\theta \to 0$ in the calculation of Josephson current, the results are still valid for an arbitrary incident direction of light. This is because the light incident from the x (y) direction causes only a much smaller shift of Weyl nodes in the k_x (k_y) direction [40] and has no effect on the Josephson current when the transport is along the z direction. Experimentally, we can use a light with a small incident angle θ. An inclined incident light can be controlled to shine only on the DSM region, without any side effect on the SC leads or FMs. It is better to modulate the chemical potential of the DSM moderately far from the Dirac points, which ensures that the bulk states make a dominant contribution over the Fermi arc surface states.

Another experimental concern is about the transport direction of the junction. It is difficult to fabricate a junction precisely aligning the z direction which connects the Dirac nodes. We argue that the main results for two-mode oscillations and 0-π transitions of a supercurrent can be easily generalized to the case of arbitrary transport direction. The 0-π transitions come from the illumination-induced splitting of Weyl nodes. And two oscillation periods are determined by the positions of Weyl nodes in the transport direction. Both two-mode oscillations and 0-π transitions will be qualitatively unchanged when the transport direction deviates from the z direction. But two oscillation periods will change and depend on the positions of Weyl nodes in the transport direction.

For the driving field, although $A_{1,2}^c$ are close, the corresponding light intensities $I_{i=1,2}^c = c\epsilon_0 (E_i^c)^2/2$ are experimentally distinguishable, where c is the speed of light, ϵ_0 is the dielectric constant, and $E_i^c \equiv \hbar \omega A_i^c / e$ is the strength of the electric component of the electromagnetic wave corresponding to A_i^c. For Cd_3As_2, the critical light intensities for $A_{1,2}^c$ are $I_1^c \approx 2.27 \times 10^{14}$ W/m^2 and $I_2^c \approx 2.45 \times 10^{14}$ W/m^2, which should be experimentally distinguishable [69–71].

IV. SUMMARY

In summary, we propose to observe the behavior of Weyl node creation and annihilation in irradiated DSMs through the Josephson signal. It is predicted that as a result of opposite-chirality ARs and equal-chirality ARs, a two-mode oscillation and 0-π transitions will be detected in the Josephson current when Weyl nodes are created by illumination-induced spin splitting. With the annihilation of one pair of Weyl nodes, the Josephson current through the SPWSM is first shut down and then recovered when two FMs at interfaces are activated. This SPWSM provides a platform for engineering anomalous Josephson φ_0 junctions with tunable ground-state phase differences. These predictions provide Josephson signatures of illumination-induced Weyl node creation and annihilation. The findings of 0-π transitions and anomalous φ_0 junctions also reveal new potentials in the application of superconducting devices based on DSMs.

ACKNOWLEDGMENTS

[1] A. H. Castro Neto, F. Guinea, N. M. R. Peres, K. S. Novoselov, and A. K. Geim, Rev. Mod. Phys. **81**, 109 (2009).

[2] N. M. R. Peres, Rev. Mod. Phys. **82**, 2673 (2010).

[3] S. Das Sarma, S. Adam, E. H. Hwang, and E. Rossi, Rev. Mod. Phys. **83**, 407 (2011).

[4] M. Z. Hasan and C. L. Kane, Rev. Mod. Phys. **82**, 3045 (2010).

[5] X.-L. Qi and S.-C. Zhang, Rev. Mod. Phys. **83**, 1057 (2011).

[6] A. Bansil, H. Lin, and T. Das, Rev. Mod. Phys. **88**, 021004 (2016).

[7] Y. Ren, Z. Qiao, and Q. Niu, Rep. Prog. Phys. **79**, 066501 (2016).

[8] N. P. Armitage, E. J. Mele, and A. Vishwanath, Rev. Mod. Phys. **90**, 015001 (2018).

[9] S. Wang, B.-C. Lin, A.-Q. Wang, D.-P. Yu, and Z.-M. Liao, Adv. Phys.: X **2**, 518 (2017).

[10] S.-Y. Xu, C. Liu, S. K. Kushwaha, R. Sankar, J. W. Krizan, I. Belopolski, M. Neupane, G. Bian, N. Ali-doust, T.-R. Chang, H.-T. Jeng, C.-Y. Huang, W.-F. Tsai, H. Lin, P. P. Shibayev, F.-C. Chou, R. J. Cava, and M. Z. Hasan, Science **347**, 294 (2015).

[11] Z. Wang, H. Weng, Q. Wu, X. Dai, and Z. Fang, Phys. Rev. B **88**, 125427 (2013).

[12] Z. K. Liu, J. Jiang, B. Zhou, Z. J. Wang, Y. Zhang, H. M. Weng, D. Prabhakaran, S.-K. Mo, H. Peng, P. Dudin, T. Kim, M. Hoesch, Z. Fang, X. Dai, Z. X. Shen, D. L. Feng, Z. Hussain, and Y. L. Chen, Nat. Mater. **13**, 677 (2014).

[13] M. Neupane, S. Y. Xu, R. Sankar, N. Alidoust, G. Bian, C. Liu, I. Belopolski, T. R. Chang, H. T. Jeng, and H. Lin, Nat. Commun. **5**, 3786 (2014).

[14] S. Borisenko, Q. Gibson, D. Evtushinsky, V. Zabolotnyy, B. Büchner, and R. J. Cava, Phys. Rev. Lett. **113**, 027603 (2014).

[15] L. Tian, G. Quinn, M. N. Ali, L. Minhao, R. J. Cava, and N. P. Ong, Nat. Mater. **14**, 280 (2015).

[16] X. Wan, A. M. Turner, A. Vishwanath, and S. Y. Savrasov, Phys. Rev. B **83**, 205101 (2011).

[17] K.-Y. Yang, Y.-M. Lu, and Y. Ran, Phys. Rev. B **84**, 075129 (2011).

[18] A. A. Burkov and L. Balents, Phys. Rev. Lett. **107**, 127205 (2011).

[19] B. Q. Lv, H. M. Weng, B. B. Fu, X. P. Wang, H. Miao, J. Ma, P. Richard, X. C. Huang, L. X. Zhao, G. F. Chen, Z. Fang, X. Dai, T. Qian, and H. Ding, Phys. Rev. X **5**, 031013 (2015).

[20] A. A. Abrikosov, Phys. Rev. B **58**, 2788 (1998).

[21] C.-X. Liu, H. J. Zhang, B. Yan, X.-L. Qi, T. Frauenheim, X. Dai, Z. Fang, and S.-C. Zhang, Phys. Rev. B **81**, 041307(R) (2010).

[22] E. Ròber, K. Hackstein, H. Coufal, and S. Sotier, Phys. Status Solidi B **93**, K99 (1979).

[23] H. B. Nielsen and M. Ninomiya, Nucl. Phys. B **185**, 20 (1981); **193**, 173 (1981).

[24] J. Cano, B. Bradlyn, Z. Wang, M. Hirschberger, N. P. Ong, and B. A. Bernevig, Phys. Rev. B **95**, 161306(R) (2017).

[25] H. Li, H. He, H. Z. Lu, H. Zhang, H. Liu, R. Ma, Z. Fan, S. Q. Shen, and J. Wang, Nat. Commun. **7**, 10301 (2016).

[26] C. Z. Li, L. X. Wang, H. Liu, J. Wang, Z. M. Liao, and D. P. Yu, Nat. Commun. **6**, 10137 (2015).

[27] J. Xiong, S. K. Kushwaha, T. Liang, J. W. Krizan, M. Hirschberger, W. Wang, R. J. Cava, and N. P. Ong, Science **350**, 413 (2015).

[28] C. L. Zhang, S. Y. Xu, C. M. Wang, Z. Lin, Z. Z. Du, C. Guo, C. C. Lee, H. Lu, Y. Feng, S. M. Huang, G. Chang, C. H. Hsu, H. Liu, H. Lin, L. Li, C. Zhang, J. Zhang, X. C. Xie, T. Neupert, M. Z. Hasan, H. Z. Lu, J. Wang, and S. Jia, Nat. Phys. **13**, 979 (2017).

[29] P. Kim, J. H. Ryoo, and C.-H. Park, Phys. Rev. Lett. **119**, 266401 (2017).

[30] C.-K. Chan and P. A. Lee, Phys. Rev. B **96**, 195143 (2017).

[31] B. J. Ramshaw, K. A. Modic, A. Shekhter, Y. Zhang, E. A. Kim, P. J. W. Moll, M. D. Bachmann, M. K. Chan, J. B. Betts, and F. Balakirev, Nat. Commun. **9**, 2217 (2018).

[32] D. R. Saykin, K. S. Tikhonov, and Y. I. Rodionov, Phys. Rev. B **97**, 041202(R) (2018).

[33] T. Kitagawa, T. Oka, A. Brataas, L. Fu, and E. Demler, Phys. Rev. B **84**, 235108 (2011).

[34] R. Wang, B. Wang, R. Shen, L. Sheng, and D. Y. Xing, Europhys. Lett. **105**, 17004 (2014).

[35] C.-K. Chan, Y.-T. Oh, J. H. Han, and P. A. Lee, Phys. Rev. B **94**, 121106(R) (2016).

[36] A. Narayan, Phys. Rev. B **94**, 041409(R) (2016).

[37] Z. Yan and Z. Wang, Phys. Rev. Lett. **117**, 087402 (2016).

[38] K. Taguchi, D.-H. Xu, A. Yamakage, and K. T. Law, Phys. Rev. B **94**, 155206 (2016).

[39] H. Hbener, M. A. Sentef, G. U. De, A. F. Kemper, and A. Rubio, Nat. Commun. **8**, 13940 (2017).

[40] P. H. Fu, H. J. Duan, R. Q. Wang, and H. Chen, Phys. Lett. A **381**, 3499 (2017).

[41] O. Deb and D. Sen, Phys. Rev. B **95**, 144311 (2017).

[42] S. Uchida, T. Habe, and Y. Asano, J. Phys. Soc. Jpn. **83**, 064711 (2014).

[43] U. Khanna, D. K. Mukherjee, A. Kundu, and S. Rao, Phys. Rev. B **93**, 121409(R) (2016).

[44] U. Khanna, S. Rao, and A. Kundu, Phys. Rev. B **95**, 201115(R) (2017).

[45] N. Bovenzi, M. Breitkreiz, P. Baireuther, T. E. O'Brien, J. Tworzydło, İ. Adagideli, and C. W. J. Beenakker, Phys. Rev. B **96**, 035437 (2017).

[46] Y. Xu, S. Uddin, J. Wang, Z. Ma, and J.-F. Liu, Phys. Rev. B **97**, 035427 (2018).

[47] A. Chen, D. I. Pikulin, and M. Franz, Phys. Rev. B **95**, 174505 (2017).

[48] D. K. Mukherjee, S. Rao, and A. Kundu, Phys. Rev. B **96**, 161408(R) (2017).

[49] H.-Y. Xie, M. G. Vavilov, and A. Levchenko, Phys. Rev. B **97**, 035443 (2018).

[50] Z. Hou and Q.-F. Sun, Phys. Rev. B **96**, 155305 (2017).

[51] S.-B. Zhang, F. Dolcini, D. Breunig, and B. Trauzettel, Phys. Rev. B **97**, 041116(R) (2018).

[52] A. Kononov, O. O. Shvetsov, S. V. Egorov, A. V. Timonina, N. N. Kolesnikov, and E. V. Deviatov, Europhys. Lett. **122**, 27004 (2018).

[53] S. Uddin, W. Duan, J. Wang, Z. Ma, and J.-F. Liu, Phys. Rev. B **99**, 045426 (2019).

[54] S.-B. Zhang, J. Erdmenger, and B. Trauzettel, Phys. Rev. Lett. **121**, 226604 (2018).

[55] B.-C. Lin, S. Wang, L.-X. Wang, C.-Z. Li, J.-G. Li, D. Yu, and Z.-M. Liao, Phys. Rev. B **95**, 235436 (2017).

[56] C.-Z. Li, C. Li, L.-X. Wang, S. Wang, Z.-M. Liao, A. Brinkman, and D.-P. Yu, Phys. Rev. B **97**, 115446 (2018).

[57] S. Wang, B.-C. Lin, W.-Z. Zheng, D. Yu, and Z.-M. Liao, Phys. Rev. Lett. **120**, 257701 (2018).

[58] A.-Q. Wang, C.-Z. Li, C. Li, Z.-M. Liao, A. Brinkman, and D.-P. Yu, Phys. Rev. Lett. **121**, 237701 (2018).

[59] B.-C. Lin, S. Wang, S. Wiedmann, J.-M. Lu, W.-Z. Zheng, D. Yu, and Z.-M. Liao, Phys. Rev. Lett. **122**, 036602 (2019).

[60] J.-F. Liu and K. S. Chan, Phys. Rev. B **82**, 184533 (2010).

[61] J.-F. Liu and K. S. Chan, Phys. Rev. B **82**, 125305 (2010).

[62] J.-F. Liu, K. S. Chan, and J. Wang, J. Phys. Soc. Jpn. **80**, 124708 (2011).

[63] J.-F. Liu, J. Phys. Soc. Jpn. **83**, 024712 (2014).

[64] J. Wang, L. Hao, and J.-F. Liu, Phys. Rev. B **93**, 155405 (2016).

[65] H. Zhang, J. Wang, and J.-F. Liu, Appl. Phys. Lett. **108**, 102601 (2016).

[66] P. A. Lee and D. S. Fisher, Phys. Rev. Lett. **47**, 882 (1981).

[67] D. S. Fisher and P. A. Lee, Phys. Rev. B **23**, 6851 (1981).

[68] U. Khanna, A. Kundu, S. Pradhan, and S. Rao, Phys. Rev. B **90**, 195430 (2014).

[69] Y. H. Wang, H. Steinberg, P. Jarillo-Herrero, and N. Gedik, Science **342**, 453 (2013).

[70] E. J. Sie, J. W. McLver, Y. H. Lee, L. Fu, J. Kong, and N. Gedik, Nat. Mater. **14**, 290 (2015).

[71] F. Mahmood, C. K. Chan, Z. Alpichshev, D. Gardner, Y. Lee, P. A. Lee, and N. Gedik, Nat. Phys. **12**, 306 (2016).